Shapes of fluid vesicles anchored by polymer chains

Kunkun Guo,† Jiafang Wang, Feng Qiu, Hongdong Zhang and Yuliang Yang*

Received 20th August 2008, Accepted 5th January 2009
First published as an Advance Article on the web 23rd February 2009
DOI: 10.1039/b814503b

We have studied polymer chains anchoring to fluid vesicles by the combination of self-consistent-field theory (SCFT) for polymer chains and Helfrich curvature energy theory for fluid membranes. Both density distributions of chain segments and shapes of fluid vesicles have been obtained. Due to the limited available space and reduced conformational entropy for the anchored polymer chains, the polymer chains induce the inhomogeneous entropic pressure on fluid membranes, which lead to the shape deformation of the vesicle. In the present study, the shapes of vesicle anchored by polymer chains for a prescribed volume and surface area are investigated as functions of interactions between chain segments and the membrane, the anchored polymer chain lengths, the solvent quality and the bending rigidity of membrane. It will be straightforward to extend this method to more complicated systems, such as vesicles with multiple anchored chains, block copolymers or semiflexible chains.

1. Introduction

Lipid bilayers are important components of living cells with diameters ranging from a few nanometres to hundreds of micrometres. In biological systems, a large number of macromolecules, such as polysaccharides, membrane proteins, glycocalix and cytoskeletons,[1,2] decorate the outer and inner sides of lipid bilayers. These macromolecules play an important role in the regulation of biological functions, such as signal transduction, endocytosis and exocytosis, cell motility, cell mitosis and protecting the cell against mechanical and chemical attacks. To study these decorated lipid bilayers, fluid vesicles anchored by polymer chains as a simplified model system have attracted wide interest in recent *in vitro* experiments.[3–8] Because of the anchoring of polymer chains to vesicles, various changes in vesicle shapes, such as budding, increnation, pearling and coiling, have been observed.

Two methods are commonly adopted to anchor polymers onto membranes: one is a chemical method *via* a lipid anchor, where one polymer is covalently bound to a lipid molecule; the other one is through physical interactions between the side groups of the polymer and the lipids.[4,5] When one polymer approaches the membrane, its conformational entropy is reduced due to the space restriction caused by the presence of the impenetrable membrane. The overall conformational entropy loss for one anchored polymer chain in an ideal state is estimated close to a few k_BT, which is far less than the anchoring energy ($\sim 20k_BT$).[16] Thus, when the polymer is anchored, the mean lifetime of the anchoring state is long so that the number of anchored polymers is approximately close to constant. However, the diffusion of a lipid anchor on membranes is much slower than shape fluctuations of vesicles, since a typical time for POPC to diffuse at a length scale is 6-fold larger than the time for shape fluctuations of vesicles to occur at the same length scale.[9,10] Likewise, the activation energy for the lateral diffusion of the anchored polymer is about $16k_BT$,[9] which is higher than the overall conformational entropy loss of the polymer. Thus, when the polymer is anchored, the anchored polymer laterally diffuses slowly enough so as to be approximately quiescent on membranes.

Numerous theoretical studies have been devoted to subtle and complicated shape changes of membranes arising from the polymer chains anchoring to membranes.[11–17] These studies have revealed that the local inhomogeneous curvature and bending rigidity of the membrane are induced by the polymer attached/adsorbed to one side of the fluid membrane.[11–17] Previous studies have suggested that polymer grafting leads to a stiffening of the membrane. However, in the case of reversible adsorption, mean field theory presents the surprising result that the adsorbed polymer decreases the bending rigidity modulus and increases the Gaussian modulus.[18,19] This contradictory result has been found for the induced curvature and rigidity of the membrane.[18,19] A different theory is proposed: because a spatial confinement of the grafted chain originates from the impenetrable membrane, the inhomogeneous pressure patch is exerted onto the membrane and the membrane shape is therefore transformed.[20,21] In addition, previous theories describe the effect of tension on the membrane shape by one parameter, an effective bending rigidity of membrane,[22,23] and ignore the fact that polymer chains could induce an inhomogeneous tension on the membrane upon interactions between the anchored chain segments and membrane.

So far, those theoretical studies focus on a polymer anchoring to a planar membrane,[11–23] which hardly explain experimental results on shape transformations of vesicles which have finite-sized and closed membrane. Recently, we have developed an approach combining Helfrich curvature elasticity theory for fluid membranes with self-consistent field theory for polymers, to explore rigid rod/polymer chains anchoring to vesicles,[24,25] and

Department of Macromolecular Science, the Key Laboratory of Molecular Engineering of Polymers, Ministry of Education, Fudan University, Shanghai, 200433, China. E-mail: yuliangyang@fudan.edu.cn
† Present address: Max Planck Institute of Colloids and Interfaces, Science Park Golm, D-14424 Potsdam, Germany

rigid rod/polymer chains anchoring to infinite membranes.[26,27] The results for polymer chains anchoring to infinite membranes[26,27] are in good agreement with those suggested by previous Monte Carlo simulations and theoretical analysis.[19–22]

Preliminary results for shapes of vesicle anchored by polymer chains have been reported briefly in a recent letter,[24] and more detail will be presented in this study. This article comprises of four parts: section II provides a detailed description of the theoretical model and numerical calculation method; section III contains vesicle shapes as a function of various factors, such as the interactions between the membrane and chain segments, the chain length, the solvent quality and the bending rigidity of the membrane, respectively. Corresponding discussions are also given based on the calculated results; finally, summaries and conclusions are drawn in section IV. Part of the algorithm to obtain the shape equation is given in the Appendix.

2. Model

The model is schematically drawn in Fig. 1. Gaussian polymer chains (n_p) with N_p segments are end-anchored to one spatial position on the membrane, and a vesicle anchored by polymer chains are placed in n_s solvent molecules. It is supposed that the vesicle membrane is impenetrable for chain segments. Note that the Kuhn statistic length of the polymer chain is assumed to be b. A single solvent molecule is approximately assumed to have the same size as the Kuhn statistic segment length b, so a single solvent molecule occupies a volume of b^3. Vesicles usually consist of amphiphilic short chains forming the lipid bilayer with a thickness about 4 nm which is comparable to the Kuhn length, and thus the lateral unit length is reasonably assumed as b. Then, the monomeric volumes $1/\rho_0$ for the polymer, vesicle and solvent are identical, the compound system is therefore homogeneous and incompressible with the reference density $\rho_0 \propto 1/b^3$.

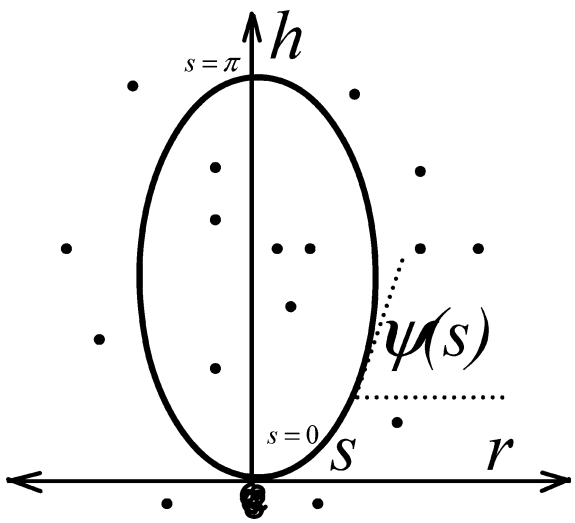

Fig. 1 A schematic illustration of polymer chains anchored to a fluid closed vesicle at $r = 0$ and $h = 0$, the solid dot indicates solvent molecules. The axis of symmetry is denoted by h. S denotes the arc-length along the contour measured from the south pole of the shape. $\psi(s)$ is the angle between the tangent to the contour and the r axis: $r = 0$, $s = 0$ in the south pole, where $r = 0$, $s = \pi$ in the north pole.

The solvent density operator is defined as $\widehat{\rho}_s(\mathbf{r}) = \sum_{i=1}^{n_s} \delta\left[\mathbf{r} - \mathbf{R}_s^i\right]$, and polymer density operator as $\widehat{\rho}_p(\mathbf{r}) = \sum_{i=1}^{n_p} \int_0^{N_p} d\tau \delta\left[\mathbf{r} - \mathbf{R}_p^i(\tau)\right]$, where $\mathbf{R}_s^i$ and $\mathbf{R}_p^i(\tau)$ represent spatial positions of solvent i and the segment τ of the ith anchored polymer chain, respectively. Solvent molecules are assumed to penetrate the membrane freely and the interaction between the membrane and solvent is then neglected. The interaction Hamiltonian βH_{int} includes the polymer–solvent molecules ($\beta V_{\text{int, }ps}$) and polymer–membrane ($\beta V_{\text{int, }pm}$) interactions, *i.e.* $\beta H_{\text{int}} = \beta V_{\text{int, }ps} + \beta V_{\text{int, }pm}$. They are given by and

$$\beta \widehat{V}_{\text{int},ps} = \chi \int d\mathbf{r}\, \widehat{\rho}_p(\mathbf{r}) \widehat{\rho}_s(\mathbf{r}) \tag{1}$$

and

$$\beta \widehat{V}_{\text{int},pm} = \eta b \oint dA \widehat{\rho}_p\{\mathbf{r} = \mathbf{R}_m(u, v)\}$$

where $\beta = k_B T$, χ and η are Flory–Huggins interaction parameters of polymer–solvent and polymer–membrane pairs, respectively. The spatial position of a vesicle $\mathbf{R}_m(u, v)$ is abbreviated as $\mathbf{R}_m$, where u, v are curvilinear coordinates for the vesicle surface.

The Hamiltonian of the polymer Gaussian chain[28] takes the form of

$$\beta H_p^0[\mathbf{R}_p] = \frac{3}{2b^2} \int_0^{N_p} d\tau \left[\frac{d\mathbf{R}_p(\tau)}{d\tau}\right]^2 \tag{2}$$

and the Hamiltonian of the membrane is formulated as[29]

$$\beta H_m^0[\mathbf{R}_m] = \frac{1}{2}\kappa \oint_{A=\mathbf{R}_m} dA[2H + c_0]^2 + \lambda \oint_{A=\mathbf{R}_m} dA + \Delta P \int_{r\in V_{in}[\mathbf{R}_m]} dV \tag{3}$$

where κ and H are the bending rigidity modulus and curvature of the fluid membrane respectively, and c_0 is the spontaneous curvature of the fluid membrane. The tensile stress λ acting on the membrane and the pressure difference $\Delta P = p_{out} - p_{in}$ across the membrane are Lagrange multipliers of vesicle surface area A and volume V, respectively.

The partition function of such a system can be written as

$$\begin{aligned}\Xi = N \frac{1}{n_s! n_p!} \int \prod_{i=1}^{i=n_s} D\mathbf{R}_s^i \int \prod_{i=1}^{i=n_p} D\mathbf{R}_p^i(\tau) \exp\{-\beta H_p^0[\mathbf{R}_p^i(\tau)]\} \\ \int D\mathbf{R}_m \exp\{-\beta H_m^0[\mathbf{R}_m]\} \exp\{-\beta \widehat{V}_{\text{int},ps} - \beta \widehat{V}_{\text{int},pm}\} \\ \prod_{\mathbf{r}} \delta\left[\rho_0 - \widehat{\rho}_p(\mathbf{r}) - \widehat{\rho}_s(\mathbf{r})\right] \delta\left[\int_{\mathbf{r}\in V_{in}[\mathbf{R}_m]} d\mathbf{r} \widehat{\rho}_p\right]\end{aligned} \tag{4}$$

where N is a constant, $\mathbf{r}\varepsilon V_{in}[\mathbf{R}_m]$ or $\mathbf{r}\varepsilon V_{out}[\mathbf{R}_m]$ represents $\mathbf{r}$ either inside or outside the vesicle, respectively. $\int D\mathbf{R}$ denotes the path integral over all possible conformations of chain segments, membrane or solvent molecules. Furthermore, the first Dirac function realizes the incompressible constraint with the reference density ρ_0, and the second Dirac function ensures polymer chains to stay outside ($\mathbf{r}\varepsilon V_{in}[\mathbf{R}_m]$). If $\mathbf{r}\varepsilon V_{out}[\mathbf{R}_m]$, the second Dirac function is valid for polymer chains inside the vesicle.

Performing Hubbard–Stratonovich transformation,[30] Lagrange multipliers, ξ is introduced to enforce the incompressible constraint, and ζ guarantees that the membrane is impenetrable by polymer chains. The external auxiliary fields $\omega_p(\mathbf{r})$ and $\omega_s(\mathbf{r})$, are self-consistent molecular fields conjugated to local densities $\rho_p(\mathbf{r})$ and $\rho_s(\mathbf{r})$, respectively. The partition function can be rewritten as

$$\Xi = N\int D\mathbf{R}_m\int D\rho_p\int D\rho_s\int D\omega_p\int D\omega_s\int D\xi\int D\zeta \exp\{-\beta F[\rho_p, \rho_s, \omega_p, \omega_s, \xi, \zeta, \mathbf{R}_m]\} \quad (5)$$

where the free energy functional is

$$\begin{aligned}\beta F\left[\rho_p, \rho_s, \omega_p, \omega_s, \xi, \zeta, \mathbf{R}_m\right] = {} & \chi\int d\mathbf{r}\rho_p\rho_s - \int d\mathbf{r}\omega_p\rho_p - \int d\mathbf{r}\omega_s\rho_s - n_p\ln Q_p \\ & - n_s\ln Q_s + \zeta\int_{r\in V_{in}[\mathbf{R}_m]} d\mathbf{r}\rho_p + \eta b\oint_{A=\mathbf{R}_m} dA\rho_p(r) \\ & - \int d\mathbf{r}\xi(\rho_0 - \rho_p - \rho_s) + \frac{1}{2}\kappa\oint_{A=\mathbf{R}_m} dA\left[2H + c_0\right]^2 \\ & + \lambda\oint_{A=\mathbf{R}_m} dA + \Delta P\int_{r\in V_{in}[\mathbf{R}_m]} dV\end{aligned} \quad (6)$$

In eqn (6), the partition function of a single polymer chain Q_p under the potential field ω_p, and the partition function of solvent molecules Q_s under the potential field ω_s are separately expressed as

$$Q_s = \int d\mathbf{r}\ \exp\{-\omega_s(\mathbf{r})\}$$

and

$$Q_p = \int d\mathbf{r} q_p(\mathbf{r}, \tau)q'_p(\mathbf{r}, \tau)$$

where the τth segment distribution function $q_p(\mathbf{r}, \tau)$ satisfies the modified diffusion equation

$$\frac{\partial}{\partial\tau}q_p(\mathbf{r}, \tau) = \frac{b^2}{6}\nabla_r^2 q_p(\mathbf{r}, \tau) - \omega_p(\mathbf{r})q_p(\mathbf{r}, \tau) \quad (7)$$

which is subjected to the initial condition $q_p[\mathbf{r} = R_m(0,0),0] = 1$ and $q_p[\mathbf{r} \neq R_m(0,0),0] = 0$ for the polymer with one end anchored to the vesicle surface $R_m(0,0)$. Due to the presence of the other free end of the anchored polymer and its lack of inversion symmetry, a conjugated segment distribution function $q'_p(\mathbf{r}, \tau)$ is subsequently introduced. The conjugated segment distribution function $q'_p(\mathbf{r}, \tau)$ satisfies a similar equation (7) with the right hand side multiplied by -1, and it obeys the initial condition $q'_p(\mathbf{r}, N_p) = 1$. In addition, this method is also valid for the polymer and vesicle compound system without any anchoring position if the initial condition is $q_p(\mathbf{r},0) = 1$.

To obtain the stable or metastable state of the system, by minimizing the free energy in eqn (6) with respect to ρ_p, ρ_s, ω_p, ω_s, ξ and ζ, respectively, we have reached the self-consistent equations for polymers and solvents,

$$\omega_p(\mathbf{r}) = \begin{cases} \eta + \chi\rho_s(\mathbf{r}) + \xi(\mathbf{r}) & r = \mathbf{R}_m \\ \zeta + \chi\rho_s(\mathbf{r}) + \xi(\mathbf{r}) & r \in V_{in}[\mathbf{R}_m] \\ \chi\rho_s(\mathbf{r}) + \xi(\mathbf{r}) & r \in V_{out}[\mathbf{R}_m] \end{cases} \quad (8)$$

$$\omega_s(\mathbf{r}) = \chi\rho_p(\mathbf{r}) + \xi(\mathbf{r}) \quad (9)$$

$$\rho_p(\mathbf{r}) = \frac{n_p}{Q_p}\int_0^{N_p} d\tau q_p(\mathbf{r}, \tau)q'_p(\mathbf{r}, \tau) \quad (10)$$

$$\rho_s(\mathbf{r}) = \frac{n_s}{Q_p}\exp\{-\omega_s(\mathbf{r})\} \quad (11)$$

$$\rho_s(\mathbf{r}) + \rho_p(\mathbf{r}) = \rho_0 \quad (12)$$

$$0 = \int_{r\varepsilon V_{in}[\mathbf{R}_m]} d\mathbf{r}\rho_p(\mathbf{r}) \quad (13)$$

According to variational algorithm given in ref. 29 and Appendix, the further minimization of the free energy βF with respect to the membrane has been performed. The shape equation of one vesicle in the presence of polymers is

$$\begin{aligned}\{\Delta P + \zeta\rho_p(\mathbf{r} = \mathbf{R}_m) + \eta b[\mathbf{n}\cdot\nabla\rho_p(\mathbf{r} = \mathbf{R}_m)]\} - 2H[\eta b\rho_p(\mathbf{r} = \mathbf{R}_m) \\ + \lambda] + 2\kappa\nabla^2 H + \kappa(2H + c_0)(2H^2 - c_0 - 2K) = 0\end{aligned} \quad (14)$$

where K is the Gaussian curvature of the membrane, $\mathbf{n}\cdot\nabla\rho_p(\mathbf{r} = \mathbf{R}_m)$ denotes the density gradient along the normal direction to the vesicle.

Compared with the general shape equation (15) derived by Ou-Yang *et al.*,[29]

$$\Delta P - 2H\lambda + 2\kappa\nabla^2 H + \kappa(2H + c_0)(2H^2 - c_0 - 2K) = 0 \quad (15)$$

three additional terms that are closely related to the spatial distribution of chain segments, are included in the shape equation (14). Firstly, the extra pressure called inhomogeneous entropic pressure $\zeta\rho_p(\mathbf{r} = \mathbf{R}_m)$ is added, which originates from a decrease of the chain conformational entropy due to the spatial confinement by the impenetrable membrane. Secondly, the interactions between chain segments and the membrane induce extra inhomogeneous tensile stress acting on the membrane that depends on the attractive or repulsive strength between chain segments and the membrane, as well as the polymer density on the membrane, *i.e.* $\eta\rho_p(\mathbf{r} = \mathbf{R}_m)$. When chain segments are adsorbed to the membrane surface, they reduce the tensile stress on the membrane contacted by chain segments. Additionally, the interactions lead to additive inhomogeneous pressure $\eta[\mathbf{n}\cdot\nabla\rho_p(\mathbf{r} = \mathbf{R}_m)]$, and this implies that more chain segments tend to cover the surface on the vesicle at the adsorptive state, $\eta < 0$, whereas less chain segments on the vesicle surface for the repulsion state, $\eta > 0$. Turning to the shape equation (14), an effective bending rigidity constant κ_{eff} that is position-dependent, can be extracted by combining the bare value κ with the induced pressure and tensile stress on the membrane. The changes in the induced pressure and tension consider the redistribution of the anchored polymer density due to the deformed membrane as well.

In numerical calculations, all parameters are dimensionless, but can be mapped to physical values. Length and energy are scaled in units of b and the bending rigidity constant κ, respectively. Then, length, surface and volume of the vesicle and the whole free energy are scaled as $\bar{\mathbf{r}} = \mathbf{r}/b$, $\bar{A} = A/b^2$, $\bar{V} = V/b^3$ and $\beta\bar{F} = \beta F/\kappa$, respectively. The bending rigidity, surface tension and pressure of the vesicle are rescaled as $\bar{\kappa} = 1k_BT$, $\bar{\lambda} = \lambda b^2/\kappa$, and $\Delta\bar{P} = \Delta P b^3/\kappa$. The dimensionless shape equation (14) has the form of

$$\left\{\Delta\bar{P}+\bar{\zeta}\frac{1}{N\kappa}\rho_p(\bar{\mathbf{r}}=\mathbf{R}_m)+\bar{\eta}b\frac{1}{N\kappa}\left[\mathbf{n}\cdot\nabla\rho_p(\bar{\mathbf{r}}=\mathbf{R}_m)\right]\right\} - 2H\left[\bar{\eta}b\frac{1}{N\kappa}\rho_p(\bar{\mathbf{r}}=\mathbf{R}_m)+\bar{\lambda}\right] + 2\bar{\kappa}\nabla^2H+\bar{\kappa}(2H+c_0)\left(2H^2-c_0-2K\right)=0 \quad (16)$$

The anchored polymers will be randomly distributed around the grafting position as shown in Fig. 1. After ensemble averaging, the vesicle shapes in the presence of the anchored polymer can be assumed to be axis symmetric and this greatly simplifies the calculation. In this present study, a vesicle anchored by polymer chains is described in the axis-symmetric coordinate system, where h is the height of the membrane and r is the coordinate along the horizontal direction. The self-consistent equations (6)–(13) and shape equation (14) are solved in the axis-symmetric coordinate system as shown in Fig. 1. In order to solve eqn (6)–(13), we set $N = 200$, $b = 1$, $\Delta\tau = 1$, $\Delta r = \Delta h = 0.05b$, with the box size $L_r = 5$ and $L_h = 20$. The initial fields $\bar{\xi}(r, h)$, $\bar{\omega}_p(r, h)$ and $\bar{\omega}_s(r, h)$ are randomly generated, and the field $\bar{\zeta}(r, h)$ is subsequently obtained based on the initial vesicle shape. Following the iterative procedure of Drolet and Fredrickson,[30] the self-consistent equations (6)–(13) are solved to obtain the polymer density $\rho_p(r, h)$ and solvent density $\rho_s(r, h)$ with these fields. According to the original vesicle shape, the resulting polymer density $\rho_p(\mathbf{r} = \mathbf{R}_m)$ and density gradient $\mathbf{n}\cdot\nabla\rho_p(\mathbf{r} = \mathbf{R}_m)$ are inserted into shape equation (14) to yield the new vesicle shape. These self-consistent equations, eqn (6)–(14), are solved iteratively to obtain the new vesicle shape as well as updated polymer density distributions. The steps are finished until the following convergence conditions have been reached between two successive iterations.

Using the Crank–Nicholson scheme and alternating-direction implicit (ADI) method, the modified diffusive equations are integrated to obtain q_p and q'_p without slope boundary condition.[31] Under the old vesicle shape, the iterative procedure of self-consistent equations will be finished until the density distributions satisfy the convergence condition of $|\rho_0 - \rho_p - \rho_s| < 1 \times 10^{-4}$. The shape equation (14) is solved to obtain the new vesicle shape with the stable polymer density $\rho_p(r, h)$.

The shooting-and-trial algorithm[32] is used to solve the shape equation (14) for an axis-symmetric vesicle. We set the step of arc length $ds = 8.0 \times 10^{-4}$, and seek for the value of $d\psi(s)/ds|_{s=0}$ until the shape closes, where $\psi(s)$ is the tilt angle between the tangent to the contour and the r direction, as shown in Fig. 1. For a given tension $\bar{\lambda}$ and pressure difference $\Delta\bar{P}$, the unalterable vesicle shape and polymer distribution have been both reached, as this iterative procedure will end when the difference for both $d\psi(s)/ds|_{s=0}$ and $\rho_p(r, h)$ between two successive iterations are less than 10^{-4}. In order to maintain the surface area $\bar{A}_0$ and volume $\bar{V}_0$ of the vesicle constant, $\bar{\lambda}$ and $\Delta\bar{P}$ are searched using successive over relation method, and the iterative procedure ends with the additive constraints of $|\bar{A} - \bar{A}_0|/\bar{A}_0 < 1 \times 10^{-4}$ and $|\bar{V} - \bar{V}_0|/\bar{V}_0 < 1 \times 10^{-4}$.

3. Result and discussion

A simple case, polymers anchoring outside or inside vesicle, is investigated at $\bar{\eta} = 0$, $c_0 = 0$ and $\bar{\chi} = 0$. The solutions of shape equation (14) contain local minima and saddle points in the space of all stationary shapes. To verify our numerical procedure, these stationary shapes of 'bare' vesicle obtained are in excellent agreement with previous results.[32] Here, shapes of fluid vesicles anchored by polymer chains are characterized by the dimensionless reduced volume $v \equiv V/[(4\pi/3)R_0^3]$, where $R_0 \equiv (A/4\pi)^{1/2}$ is the radius of a sphere with the same surface area. With decreasing reduced volume v, the biconcave character of a isolate cell becomes more pronounced, giving that $v = 1$ is for spherical object, v in the range 0.9–1 has an approximately prolate ellipsoidal shape and $v = 0.6$ corresponds to the normal human erythrocyte.

Several typical shapes of the vesicle anchored by polymer, and the 'bare' vesicles with the same reduced volume v are illustrated in Fig. 2 with the anchored polymer outside ($\bar{\zeta} > 0$) and in Fig. 3 with the anchored polymer inside ($\bar{\zeta} < 0$). As mentioned above, $b = 5$ nm. The coil size of the polymer chains is close to $\sqrt{N}b \approx 70$ nm with $N = 200$ (note that in all figures the length is rescaled by b and the density of the polymer chains is drawn in a gray scale on a logarithmic scale). In Fig. 2 and 3, the combined Helfrich–SCFT approach leads to a variety of interesting shapes, such as prolates, oblates, discocytes and stomatocytes. Due to local disturbances of these anchored polymer chains, the symmetry of the 'bare' shapes is destroyed, for example the spherical shape is unstable and thus are not observed any more. Complete phase diagram will be presented in a later work, giving the shape of the lowest bending energy for a given v, spontaneous curvature c_0 and other parameters.

Next, we study shape transformations of a vesicle anchored by polymer chains with invariable surface area and volume. The surface area and volume of vesicles presented in this study correspond to the physical magnitude of 0.026 μm^2 and 0.34 × 10^{-3} μm^3, respectively. Shapes of vesicles anchored by polymer chains are presented in Fig. 4 upon interaction parameter $\bar{\eta}$ varying from $\bar{\eta} = 10$ (repulsion) to $\bar{\eta} = -25$ (adsorption). As shown in Fig. 4(a), the 'bare' sphere vesicle becomes prolate at $\bar{\eta} = 0$, whereas the vesicle transforms from prolate to oblate with further decreasing interaction parameter $\bar{\eta}$. A notable feature in Fig. 4(a) is that at $\bar{\eta} = -25$, two small protrusions are observed in the south and north poles of the vesicle. It is also seen in Fig. 4 that these vesicles are drawn out along the perpendicular direction (h axis) when $\bar{\eta} > 0$, but are pressed along h direction and become broader along r direction when $\bar{\eta} < 0$. To gain more insights into these transformations, the bending elastic energy of vesicles is studied. With a decrease of the interaction parameters $\bar{\eta}$, the bending elastic energy of these vesicles is slightly changed. The scope of the bending energy is $|F_{\{de,\,b\}} - F_{\{ad,\,b\}}|/F_{\{de,\,b\}} < 0.05$, where $F_{\{de,\,b\}}$ represents the bending elastic energy of the vesicle at $\bar{\eta} = 10$ and $F_{\{ab,\,b\}}$ at $\bar{\eta} = -25$. Thus, the transitions among these shapes are easily realized, which have been observed in recent experiments.[33] In addition, the bending elastic energy of the 'bare' vesicles shown in Fig. 4(b) is the same as that in Fig. 4(c), but the bending elastic energy of the vesicles anchored by polymers in Fig. 4(b) increases slightly faster than those in Fig. 4(c) with the same interaction parameter $\bar{\eta}$. Compared to Fig. 4(c), the membranes in Fig. 4(b) provide less active space for the anchored polymers, the conformational entropy of polymers is more reduced and the bending energy of the vesicles increases as well.

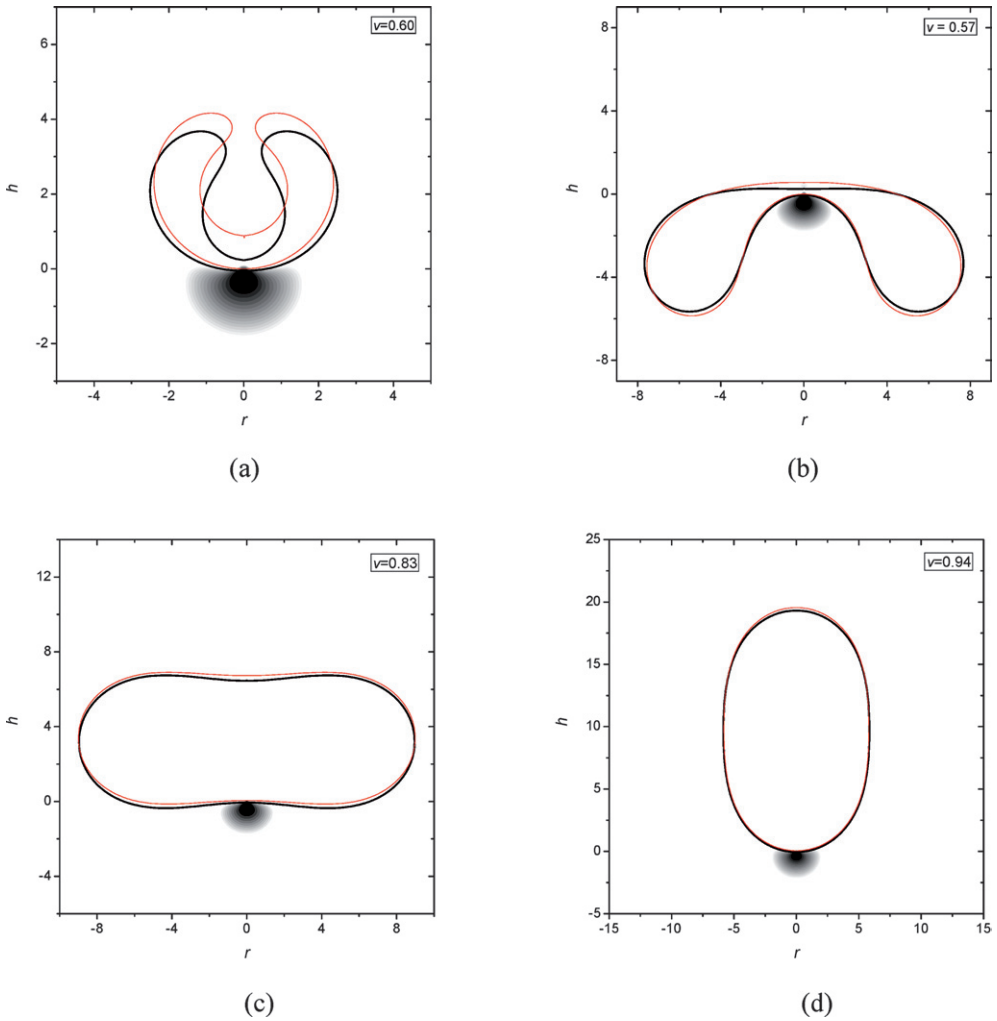

Fig. 2 Typical stationary solutions, including shapes of the vesicle and segment distributions of the polymer chain, to the self-consistent equations. The shape of the vesicle with polymer anchored outside is represented by black solid curves and the density of the polymer chain is drawn in gray scale map by logarithm scale. The shape of the 'bared' vesicle is represented by red curves. The horizontal (r) and vertical (h) axes are scaled by b. In all cases, we use $b = 1$, $N = 200$, $\kappa = 1.67$, $c_0 = 0$, $\bar{\chi} = 0$, $\bar{\eta} = 0$ and $\bar{\zeta} = 300$.

Besides the shapes of the vesicles, polymer density distributions are also significantly changed upon interactions between chain segments and the membrane. When $\bar{\eta} \geq 0$, as anticipated, the polymers are repelled from the vesicle surface, and thus have the form of a mushroom with a size comparable to the dissolved polymers, as given in the left insets of Fig. 4(a)–(c). $\bar{\eta} < 0$ means adsorption interactions between chain segments and the membrane. Weak adsorption leads the polymers to form squashed mushroom shapes. The strong adsorption interactions play dominating roles over the conformational entropy loss of the polymers, and the vesicle is so 'starved' that the chain segments form 'pancakes' which are tightly bound onto the membrane surface, as shown in the right insets of Fig. 4. As expected, the chain segments on the vesicle surface go up 3.5 times when $\bar{\eta}$ decreases from 10 to -25, and the lateral size of the polymers, as one of important factors of the membrane's curvature,[16,17] decreases close to 0.2 R_p (the end-to-end distance) at $\bar{\eta} = -25$. Thus, both the chain segments distribution and lateral size of the polymers are significantly changed upon interactions ($\bar{\eta}$) between chain segments and the membrane.

Without the anchoring position between the planar membrane and chain segments, analytical results show that at weak adsorption between the membrane and chain segments, the membrane will bend away from chain segments so as to provide more active spaces and reduce the entropic loss of the polymer,[11,15] whereas at strong adsorption, the membrane will bend towards chain segments to increase the contact area. However, for the planar membrane anchored by the polymer with the anchoring position, different results have been obtained in that the membrane always bends away from the polymer even in the strong adsorption.[15,16] In this study, at strong adsorption ($\bar{\eta} = -25$), the vesicles mildly bend away from the chain segments as shown in Fig. 4(b). Whereas, Fig. 4(a) and (c) show that the vesicle curvature near the anchoring position is kept almost unchanged even with vesicle shape deformed remarkably at $\bar{\eta} = -25$. Therefore, the membrane neither increases the contact area nor provides more active spaces for the anchored polymers. These results are counterintuitive but reasonable, because the membrane at first has to ensure its closure and finite size, and then chooses to adjust its shape to attain the balance of the global

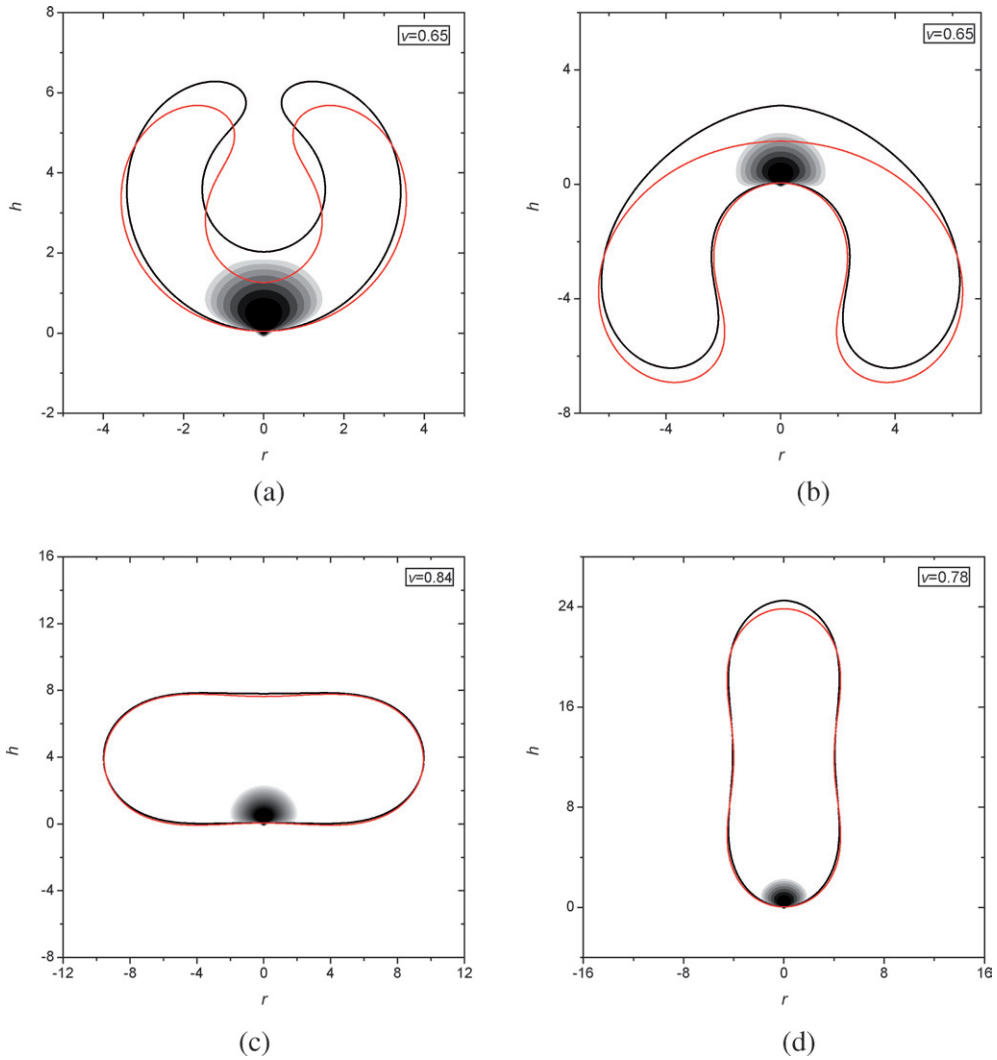

Fig. 3 Typical stationary solutions, including shapes of the vesicle and segment distributions of the polymer chain, to the self-consistent equations. The shape of the vesicle with polymer anchored inside is represented by black solid curves and the density of the polymer chain is drawn in gray scale map by logarithm scale. The shape of the 'bared' vesicle is represented by red curves. The horizontal (r) and vertical (h) axes are scaled by b. In all cases, we use $b = 1$, $N = 200$, $\kappa = 1.67$, $c_0 = 0$, $\bar{\chi} = 0$, $\bar{\eta} = 0$ and $\bar{\zeta} = -300$.

free energy, such as interactions between chain segments and the membrane, the conformational entropy loss for the polymers and the bending elastic energy for the vesicle. Turning to the shape, equation (14), when $\bar{\eta} < 0$, the polymer density on the membrane surface increases with decreasing $\bar{\eta}$, thus causing the increased inhomogeneous entropic pressure $\zeta\rho_p(\mathbf{r} = \mathbf{R}_m)$. However, the additive pressure $\eta[\mathbf{n}\cdot\nabla\rho_p(\mathbf{r} = \mathbf{R}_m)]$, which arises from adsorption interactions between the membrane and chain segments, can counteract the induced inhomogeneous entropic pressure $\zeta\rho_p(\mathbf{r} = \mathbf{R}_m)$. These results deeply reveal that shape changes are subtle and intricate for the finite-sized and closed vesicle. It depends not only on local interactions between chain segments and the membrane, but also on the global shape of the vesicle.

The Flory–Huggins interaction parameter χ between chain segments and solvents is ideally expected to influence the conformational distribution of chain segments, despite it is absence in the shape equation (14). Fig. 5 presents shapes of vesicles anchored by polymer chains when $n_p = 200$, $\bar{\chi} = 0$ or $\bar{\chi} = 160$. It is seen from Fig. 5 that these two vesicle shapes are indistinguishable. However, the locally magnified shapes (the north pole of the vesicle) in the top-left inset of Fig. 5 show that when $\bar{\chi}$ increases from $\bar{\chi} = 0$ to $\bar{\chi} = 160$, the height of the vesicle increases slightly. Therefore, the quality of solvents contributes slightly to the shape deformation of a vesicle. As far as the polymer density distribution is concerned, these two mushrooms at the $\bar{\chi}$ values are very similar. Likewise, the polymer densities along the h direction at $r = 0$ are presented in the top-right inset of Fig. 5. When interaction parameter $\bar{\chi}$ increases from 0 to 160, the polymer density clearly goes up beyond the end-to-end distance (R_p). However, the polymer density on the vesicle surface increases only 20%, because the highest density is close to the membrane surface ($h = 0$). Accordingly, the differences in both polymer densities and deformed shapes are too small to discern. Further increasing $\bar{\chi}$ will cause chain segments to collapse, which is difficult for self-consistent field theory. Previous scaling theory has suggested that the induced curvature

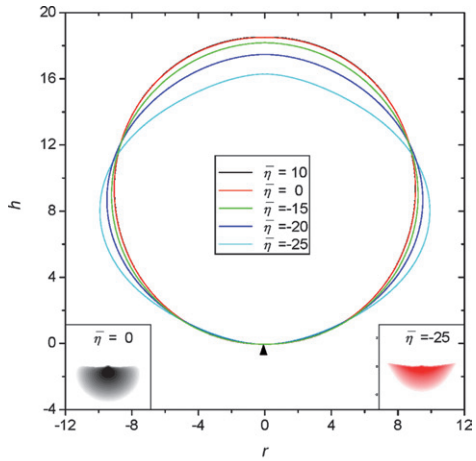

(a)

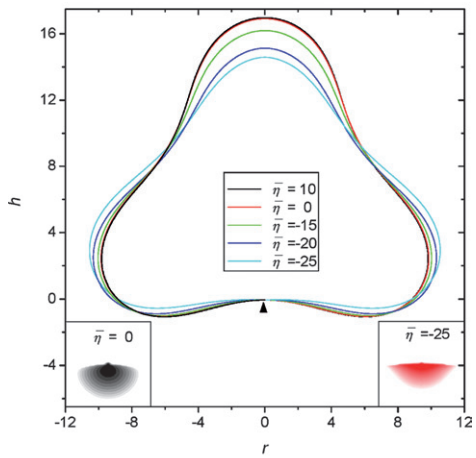

(b)

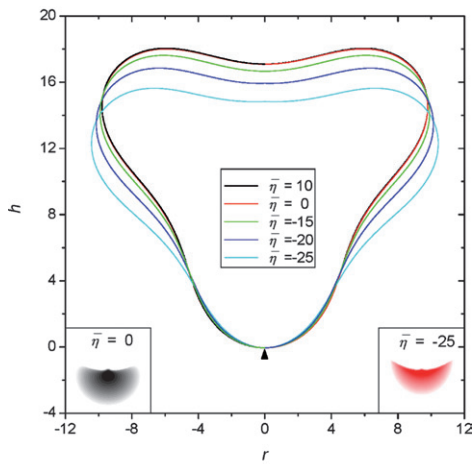

(c)

Fig. 4 Effect of the polymer–membrane interaction parameter, $\bar{\eta}$. The parameters used are $c_0 = 0$, $\bar{\chi} = 0$, $\kappa = 25$ and $\bar{\zeta} = 300$. The shape of the vesicle is represented by different type curves and the anchoring points are indicated by arrows.

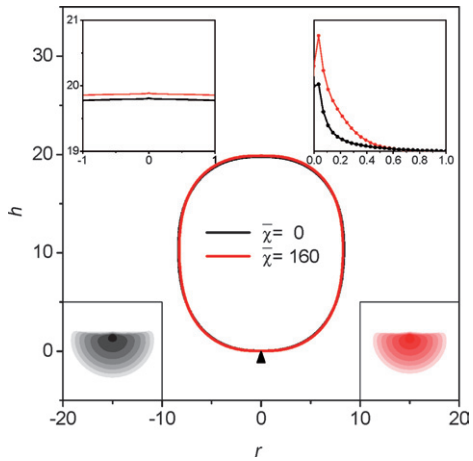

Fig. 5 The effect of the polymer-solvent interaction parameter, $\bar{\chi}$. The parameters used are $c_0 = 0$, $\bar{\eta} = 0$, $\kappa = 2$ and $\bar{\zeta} = 300$. For clarity, the anchoring points are indicated by arrows. Membrane shapes are magnified in the north pole in the left inset, polymer densities of $r = 0$ are listed in the right inset and the horizontal axis is scaled by R_p.

M_{pi} is proportional to the coverage $\bar{\Gamma}$ of polymer.[16,17] Likewise, the alterations of R_p and $\bar{\Gamma}$ shown in Fig. 5 are less as a function of the solvent quality, thus both the bending elastic energy and shapes of the vesicle are kept almost unchangeable within certain range of $\bar{\chi}$. We can conclude that the effect of $\bar{\chi}$ on vesicle shapes can be disregarded compared with other parameters. In addition, the anchored polymer has a self-avoiding random walk configuration at $\bar{\chi} = 0$.

The chain length of the anchoring polymers is relevant to polymer densities adjacent to the membrane, and is therefore expected to influence the shape transformation of a vesicle. Fig. 6 gives the shapes of vesicles anchored by polymers influenced by chain lengths at $\bar{\eta} = 0$ and $\bar{\eta} = -15$. At $\bar{\eta} = 0$, the vesicle shapes are almost unchanged, and only a slight effect of the chain length on the vesicle is observed. At $\bar{\eta} = -15$, vesicle shapes are all pressed along the perpendicular direction (h axis). However, vesicle shapes change gradually as the chain length of the anchored polymers increases. To provide insights into shape transformation of vesicles, the polymer density distribution has to be studied since the induced entropic pressure and tensile stress depend on the polymer density on the membrane surface. At $\bar{\eta} = -15$, the polymer density near the membrane surface at first increases rapidly and then much slower as a function of the chain length. With the increasing chain length, the membrane will already be full of chain segments and is not able to 'eat' any more chain segments at this specific adsorptive state. At $\bar{\eta} = 0$, the polymer density near the membrane surface is almost independent of the anchored polymer length. It is also found that for the grafted polymer with the same grafted density, the polymer density adjacent the grafted surface remains almost unchanged with repulsive interactions between the grafted surface and polymer, disregarding to the chain length of the grafted polymer.[34] Then, we can conclude that when $\bar{\eta} \geq 0$, the polymer density near the membrane surface is unalterable with a increase of the anchored chain length, and then the induced pressures $\{\zeta\rho_p(\mathbf{r} = \mathbf{R}_m)$ and $\eta[\mathbf{n}\cdot\nabla\rho_p(\mathbf{r} = \mathbf{R}_m)]\}$ and tensile stress $[\eta\rho_p(\mathbf{r} = \mathbf{R}_m)]$ are kept unchanged in this system. Thus, shape deformation

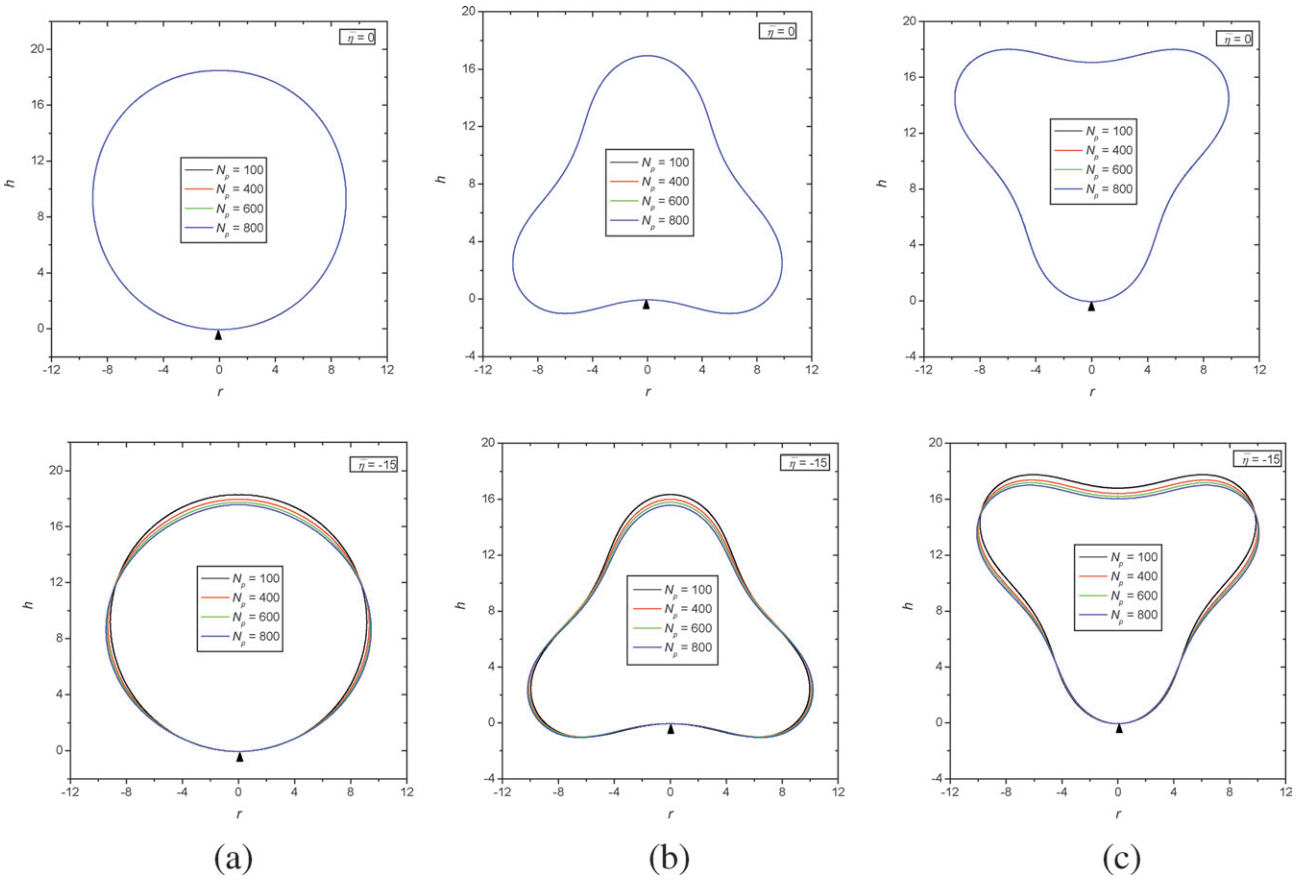

Fig. 6 The effect of the polymer-chain length parameter, n_p. The parameters used are $c_0 = 0$, $\bar{\chi} = 0$, $\kappa = 25$, and $\bar{\zeta} = 300$.

of the vesicle is always independent of the chain length when $\bar{\eta} \geq 0$, whereas the vesicle shape is at first influenced strongly and then weakly as the chain length increases when $\bar{\eta} < 0$.

The bending rigidity is one of the basic parameters of fluid membranes and can be measured by means of the micropipette method.[35,36] For biological membranes primarily composed of a phospholipids bilayer, the bending rigidity constant κ ranges typically from $10k_BT$ to $40k_BT$, and is much smaller than that of the vesicle consisting of amphiphilic polymers.[35,36] The bending rigidity modulus describes a kind of capability for a vesicle that can resist perturbations and deformations. In Fig. 7, shapes of vesicles anchored by polymers are presented as a function of the bending rigidity constant κ at $\bar{\eta} = 0$ and $\bar{\eta} = -15$. As shown in Fig. 7, significant changes in vesicle shapes are observed, and the vesicles approach a 'bare' vesicle when the bending rigidity increases from $\kappa = 5$ to $\kappa = 100$. This implies that vesicles with less bending rigidity are prone to fluids, susceptible to extra-pressure and tensile stress, and will be seriously deformed. In addition, Fig. 7(b) shows that when the bending rigidity constant κ shifts from 100 to 5, serious changes in the vesicle shapes are observed at $\bar{\eta} = -15$ whereas the vesicle shapes at $\bar{\eta} = 0$ are kept almost unchanged. Thus, the vesicle will respond differently to the increase of the bending rigidity constant and adjust its shape according to its globe factors, including interactions between membrane and chain segments, the bending elastic energy for the closed and finite-sized vesicles, *etc*.

4. Conclusion

Shapes of fluid vesicles anchored by polymer chains are studied *via* a combination of Helfrich curvature elastic theory for fluid membranes with self-consistent field theory for polymers. The approach not only leads to stable and metastable shapes of the vesicle but also produces the density distribution of chain segments. Due to the vesicle's impenetrability to polymer chains, the available space for the polymer is reduced. Thus, the anchored polymer chains induce the inhomogeneous entropic pressure on the membrane and cause the deformation of the vesicle shape. When adsorptive or repulsive interactions are found between the vesicle membrane and chain segments, the anchored polymers not only lead to the inhomogeneous pressure on the membrane but also change the local tension of the membrane so as to deform the vesicle remarkably. Likewise, conformations of the anchored polymer chains undergo a transition from 'mushroom' to 'pancake' with the increase of the adsorption strength. Furthermore, the effects of the chain length of anchored polymers and the bending rigidity on the vesicle deformation are explicitly investigated. The chain length of anchored polymers hardly changes the vesicle shape when $\bar{\eta} \geq 0$, whereas the effect of the chain length is at first enhanced rapidly and then slowly when $\bar{\eta} < 0$. High bending rigidity of the membrane can resist extra inhomogeneous pressure and tension, and then the vesicle exhibits much less transformation. In addition, the solvent quality scarcely affects the density distribution

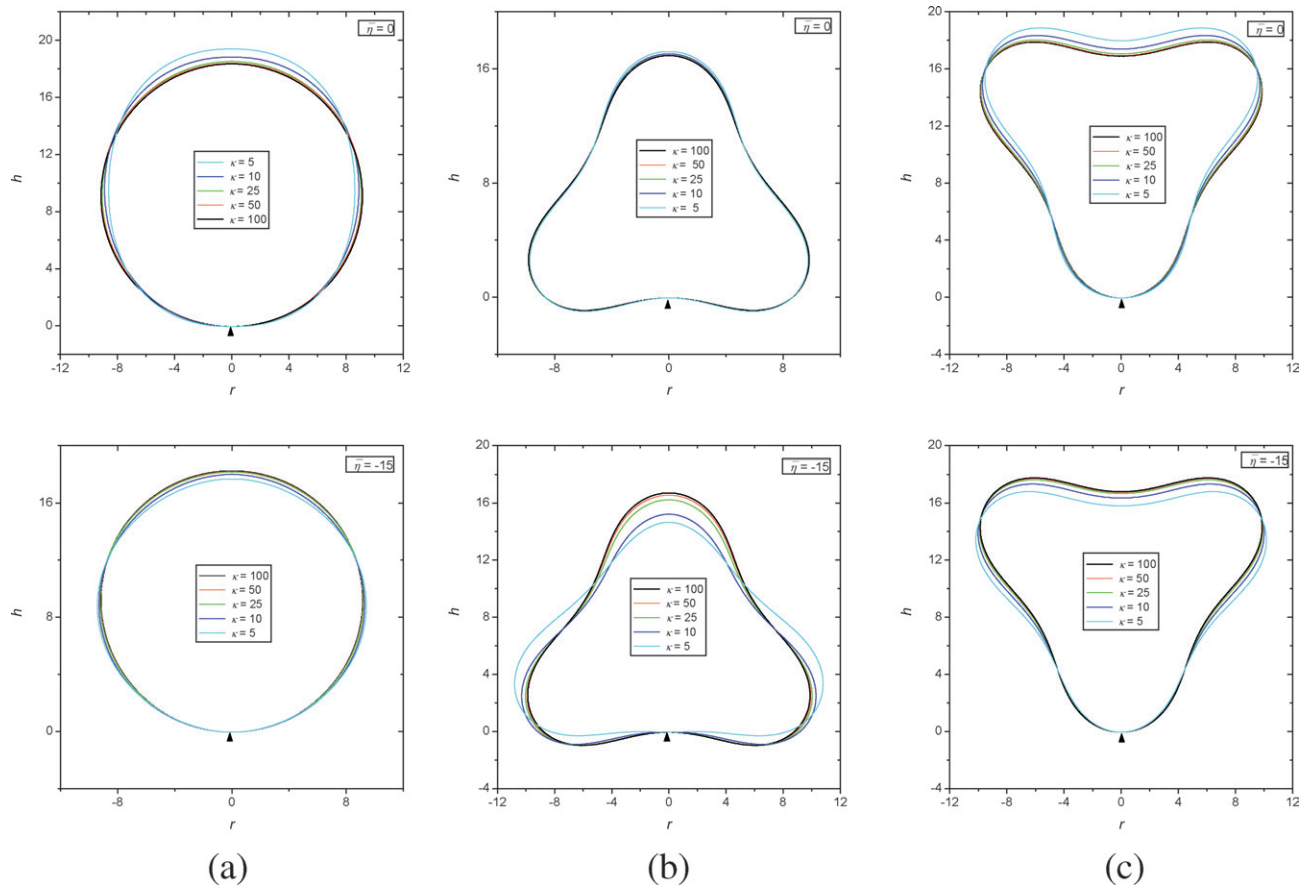

Fig. 7 The effect of the bending rigidity parameter, κ. The parameters used are $c_0 = 0$, $\bar{\chi} = 0$, and $\bar{\zeta} = 300$.

of chain segments and its effect of solvent quality on the shape of the vesicle is approximately neglected compared with other parameters. The results presented here provide valuable insights to various biological processes, including cell motility, cell shape, cell functions, *etc.*

Appendix

Since the vesicle we studied is assumed to be one component, the normal direction has to be considered and the tangential direction can be reasonably neglected when the free energy functional in eqn (6) is minimized with respect to the membrane. The variation algorithm can be referred to in the book by Ou-Yang *et al.*[29] and the terms relevant to the polymer density will be given as follows.

The vesicle shape after a small fluctuation can be described as, $R'_m(u, v) = R_m(u, v) + \varphi(u, v)\mathbf{n}$, where $\mathbf{n}$ is normal direction and $\varphi(u, v)$ is continuous function of u, v. The expansion of the term, $\int_{\mathbf{r}\in V[R_m]} d\mathbf{r}\rho_p$, is given by

$$\delta_\perp\left\{\int_{r\in V[R_m(u,v)]} dr\rho_p\right\} = \int_{r\in V\left[R'_m(u,v)\right]} dr\left(\rho_p+\delta\rho_p\right) - \int_{r\in V\left[R_m(u,v)\right]} dr\rho_p$$
$$= \int_{r\in V\left[\varphi(u,v)\mathbf{n}\right]} dr\left(\rho_p+\delta\rho_p\right) + \int_{r\in V\left[R_m(u,v)\right]} dr\delta\rho_p \tag{17}$$

The last term in the right-hand of the equation (17) is close to zero and can be therefore neglected. The equation (17) takes the form

$$\int_{r\in V[\varphi(u,v)\mathbf{n}]} dr\left(\rho_p+\delta\rho_p\right)$$
$$\simeq \int_{r\in V[\varphi(u,v)\mathbf{n}]} dr\rho_p$$
$$= \int_{u,v}\int_0^{\varphi(u,v)} \rho_p[R_m(u,v)+\tau\mathbf{n}]g^{1/2}[R_m(u,v)+\tau\mathbf{n}]d\tau dudv$$
$$= \int_{u,v}\int_0^{\varphi(u,v)} \left[\rho_p(u,v)+\nabla\rho_p(u,v)\cdot\tau\mathbf{n}\right]\left[g^{1/2}(u,v)-2Hg^{1/2}(u,v)\tau\right]d\tau dudv$$
$$= \int_{u,v}\int_0^{\varphi(u,v)} \left[\rho_p(u,v)g^{1/2}+\left(\nabla\rho_p(u,v)\cdot\mathbf{n}g^{1/2}-2H\rho_p(u,v)g^{1/2}\right)\tau\right]d\tau dudv$$
$$-\int_{u,v}\int_0^{\varphi(u,v)} 2Hg^{1/2}\nabla\rho_p(u,v)\cdot\mathbf{n}\tau^2 d\tau dudv$$
$$= \int_{u,v}\left[\rho_p(u,v)g^{1/2}\varphi+\frac{1}{2}\left(\nabla\rho_p(u,v)\cdot\mathbf{n}g^{1/2}-2H\rho_p(u,v)g^{1/2}\right)\varphi^2\right]dudv$$
$$-\int_{u,v}\frac{2}{3}Hg^{1/2}\nabla\rho_p(u,v)\cdot\mathbf{n}\varphi^3 dudv$$
$$\simeq \int_{u,v}\rho_p(u,v)g^{1/2}\varphi dudv \tag{18}$$

In eqn (18), $\rho_p[R_m(u, v)]$ is simplified to symbol as $\rho_p(u, v)$, where $\varphi(u, v)$ is an arbitrary, sufficiently and well smooth function of u and v, whereas τ is a smaller continuous, smooth function than $\varphi(u, v)$.

Accordingly, a similar variation of the term $\oint_{A=R_m} dA\rho_p$ can be achieved and is given by

$$\begin{aligned}
&\delta_\perp \int_{u,v} \rho_p g^{1/2} du dv \\
&= \int_{u,v} \rho_p[R_m(u,v) + \varphi \mathbf{n}]\left(g^{1/2} + \delta g^{1/2}\right) du dv - \int_{u,v} \rho_p(u,v) g^{1/2} du dv \\
&= \int_{u,v} \left\{ \left[\rho_p[R_m(u,v) + \varphi \mathbf{n}] - \rho_p[R_m(u,v)]\right] g^{1/2} + \rho_p[R_m(u,v) + \varphi \mathbf{n}] \delta g^{1/2} \right\} du dv \\
&= \int_{u,v} \left\{ \nabla \rho_p \cdot \varphi \mathbf{n} g^{1/2} + \left[\rho_p(u,v) \delta g^{1/2} + \nabla \rho_p \cdot \varphi \mathbf{n} \delta g^{1/2}\right] \right\} du dv \\
&= \int_{u,v} \left\{ \nabla \rho_p \cdot \mathbf{n} \varphi - 2H \rho_p(u,v) \varphi - 2H \nabla \rho_p \cdot \mathbf{n} \varphi^2 \right\} g^{1/2} du dv \\
&\simeq \int_{u,v} \left\{ \nabla \rho_p \cdot \mathbf{n} - 2H \rho_p(u,v) \right\} g^{1/2} \varphi du dv
\end{aligned} \tag{19}$$

Acknowledgements

Dr Kunkun Guo thanks Jianfeng Li for helpful discussions. We gratefully acknowledge financial support from National Basic Research Program of China (Grant No. 2005CB623800).

References

1 R. Lipowsky and E. Sackmann, *Structure and Dynamics of Membranes, Vol. 1 of Handbook of Biological Physics*, Elsevier, Amsterdam, 1995.
2 H. G. Doebereiner, E. Evans, M. Krauss, U. Seifert and M. Wortis, *Phys. Rev. E*, 1997, **55**, 4458.
3 I. Tsafrir, D. Sagi, T. Arzi, M. A. Guedeau-Boudeville, V. Frette, D. Kandel and J. Stavans, *Phys. Rev. Lett.*, 2001, **86**, 1138.
4 Szleifer, O. V. Gerasimov and D. H. Thompson, *Proc. Natl. Acad. Sci.*, 1998, **95**, 1032.
5 Tsafrir, M. A. Guedeau-Boudeville, D. Kandel and J. Stavans, *Phys. Rev. E*, 2001, **63**, 031603.
6 V. Nikolov, R. Lipowsky and R. Dimova, *Biophys. J.*, 2007, **92**, 4356.
7 V. Frette, I. Tsafrir, M. A. Guedeau-Boudeville, D. Kandel and J. Stavans, *Phys. Rev. Lett.*, 1999, **83**, 2465.
8 I. Tsafrir, Y. Caspi, T. Arzi and J. Stavans, *Phys. Rev. Lett.*, 2003, **91**, 138102.
9 H. C. Gaede and K. Gawrisch, *Biophys. J.*, 2003, **85**, 1734.
10 A. G. Zilman and R. Granek, *Phys. Rev. Lett.*, 1996, **77**, 4788.
11 C. Hiergeist and R. Lipowsky, *J. Phys. II (France)*, 1996, **6**, 1465.
12 P.-G. de Gennes, *Scaling Concepts in Polymer Physics*, Cornell University Press, New York, 1979.
13 Y. W. Kim and W. Sung, *Phys. Rev. E*, 2001, **63**, 041910.
14 T. Auth and G. Gompper, *Phys. Rev. E*, 2003, **68**, 051801.
15 M. Breidenich, R. R. Netz and R. Lipowsky, *Eur. Phys. J. E*, 2001, **5**, 403.
16 R. Lipowsky, *Europhys. Lett.*, 1998, **30**, 197.
17 R. Lipowsky, H. G. Doebereiner, C. Hiergiest and V. Indrani, *Physica A*, 1998, **249**, 536.
18 F. Clement and J.-F. Joanny, *J. Phys. II (France)*, 1997, **7**, 973.
19 J. Brooks, C. Marques and M. Cates, *J. Phys. II (France)*, 1991, **1**, 673.
20 T. Bickel, C. Jeppesen and C. M. Marques, *Eur. Phys. J. E*, 2001, **4**, 33.
21 T. Bickel, C. M. Marques and C. Jeppesen, *Phys. Rev. E*, 2000, **62**, 1124.
22 T. Bickel and C. M. Marques, *Eur. Phys. J. E*, 2002, **9**, 349.
23 T. Auth and G. Gompper, *Phys. Rev. E*, 2005, **72**.
24 J. F. Wang, K. K. Guo and Y. L. Yang, *Phys. Rev. E*, 2005, **71**, 041908.
25 M. Z. Sun, F. Qiu and Y. L. Yang, *J. Phys. Chem. B*, 2006, **110**, 9698.
26 K. K. Guo, F. Qiu and Y. L. Yang, *J. Chem. Phys.*, 2005, **123**, 074906.
27 K. K. Guo, F. Qiu, H. D. Zhang and Y. L. Yang, *Acta. Phys. Sinica*, 2006, **55**, 155.
28 M. Doi and S. F. Edwards, *The Theory of Polymer Dynamics*, Oxford University Press, United States, 1986.
29 Z. -C. Ou-Yang, J. -X. Liu, Y. -Z. Xie, *Geometric Methodsin the Elastic Theory of Membranes in Liquid Crystal Phases*, World Scientific Press, Singapore, 1999.
30 F. Drolet and G. H. Fredrickson, *Phys. Rev. Lett.*, 1999, **83**, 4317.
31 Here, no flux boundary condition are $\partial q/\partial r|_{r=L_r} = 0$ and $\partial q/\partial h|_{r=L_h} = 0$, the same with q'.
32 U. Seifert, K. Berndl and R. Lipowsky, *Phys. Rev. A*, 1991, **44**, 1182.
33 F. Quemeneur and A. Rammal, *Biomacromolecules*, 2007, **8**, 2512.
34 S. T. Milner, *Science*, 1991, **251**, 905.
35 R. Bar-Ziv and E. Moses, *Phys. Rev. Lett.*, 1994, **73**, 1392.
36 E. Evans and W. Rawicz, *Phys. Rev. Lett.*, 1997, **79**, 2379.